

Statistical Properties of Linear Antenna Impedance in an Electrically Large Cavity

Larry K. Warne, Kelvin S. H. Lee, H. Gerald Hudson, William A. Johnson, *Senior Member, IEEE*, Roy E. Jorgenson, *Member, IEEE*, and Stephen L. Stronach

Abstract—This paper presents models and measurements of linear antenna input impedance in resonant cavities at high frequencies. Results are presented for both the case where the cavity is undermoded (modes with separate and discrete spectra) as well as the overmoded case (modes with overlapping spectra). A modal series is constructed and analyzed to determine the impedance statistical distribution. Both electrically small as well as electrically longer resonant and wall mounted antennas are analyzed. Measurements in a large mode stirred chamber cavity are compared with calculations. Finally a method based on power arguments is given, yielding simple formulas for the impedance distribution.

Index Terms—Antenna measurements, antenna theory, cavities, cavity resonators, chaos, impedance, resonance, statistics.

I. INTRODUCTION

IN THIS PAPER, statistical models for the input impedance Z_{in} of a linear antenna in an electrically large cavity are developed [1]. Cases where modes have overlapping spectra, and the antenna impedance approaches the free space value [2], as well as separate discrete spectra [3], [4] are both considered. The behavior of the impedance and its extreme values are useful in determining the transmission and reception characteristics of an antenna and practical bounds for these quantities. An electrically short center driven dipole is treated first by means of a modal series for the cavity field. The statistical properties of the high-frequency cavity field are introduced [7], [10], [11] from which distributions for the impedance are extracted by means of Monte Carlo simulation and asymptotic analysis. These simulations and asymptotic results are compared to measurements in a mode stirred chamber. It is then shown how these results apply to an electrically longer resonant dipole and a wall-mounted monopole antenna. The known enhancement of the field near the cavity wall [24] is found to correspond to the behavior of the field correlation function, which is needed in the treatment of the monopole antenna. Finally, a simplified approach using conservation of power is carried out that yields practically useful formulas for the impedance distributions and extreme values.

Manuscript received January 4, 2001; revised November 14, 2001. "Sandia" is a multiprogram laboratory operated by Sandia Corporation, a Lockheed Martin Company, for the U.S. Department of Energy under Contract DE-AC04-94AL85000.

L. K. Warne, H. G. Hudson, W. A. Johnson, R. E. Jorgenson, and S. L. Stronach are with Sandia National Laboratories, Albuquerque, NM 87185-1152 USA (e-mail: lkwarne@sandia.gov).

K. S. H. Lee is with ITT Industries/AES, Los Angeles, CA 90024 USA.
Digital Object Identifier 10.1109/TAP.2003.811483

II. ELECTRICALLY SHORT ANTENNA

We use the potential representations for the field in the Coulomb gauge similar to those in Smythe [4]; however, the finite wall conductivity is introduced differently, consistent with the approach in Collin [5] (derivations can be found in [1] and a summary in the Appendix). The electrically short center driven dipole, aligned with the z axis, has current distribution $I(z) \sim I(0)(1 - |z|/h)$. Using this in the equations (69), (74), (75), (77), and (78) of the Appendix, with time dependence $e^{-i\omega t}$, gives the input impedance

$$Z_{in} \sim R - iX + R_{rad} \sum_n \left(\frac{2\pi Q}{k^3 V} \right) \frac{(i\omega^2/Q) \omega^2/\omega_n^2}{\omega^2(1 + i/Q) - \omega_n^2} 3A_{nz}^2(r) \quad (1)$$

where R_{rad} is the antenna radiation resistance in free space which, for a short dipole of length $2h$ with triangular current distribution, is [6]

$$R_{rad} \sim \frac{\eta_0}{6\pi} (kh)^2. \quad (2)$$

The quantity $\eta_0 \approx 120\pi$ ohms is the impedance of free space and $k = \omega/c$ is the wavenumber (c is the vacuum velocity of light). The quantity

$$Z = R - iX \quad (3)$$

is the local impedance of the antenna, consisting of the ohmic resistance R and local reactance X [this includes the quasistatic part due to the cavity but can be approximated as the free space value consistent with (75), and with (77)]

$$X \sim -1/(\omega C) + \omega L. \quad (4)$$

The capacitance is dominant for a short dipole, with [6]

$$C \sim \frac{2\pi\epsilon_0 h}{\Omega_e} \quad (5)$$

where the expansion parameter is

$$\Omega_e = \Omega - 2(1 + \ln 2) \quad (6)$$

and the antenna fatness parameter is $\Omega = 2\ln(2h/a)$. The inductance is found to be

$$L \sim \frac{\mu_0 h}{2\pi} \frac{1}{3} (\Omega_e + \text{constant}) \quad (7)$$

where the leading term Ω_e is correct but the constant $= 6\ln 2 - 8/3 \approx 3/2$ is slightly different than the proper first order term $2/3$ (this first order inductance result can be corrected by retaining a higher order frequency term in the current distribution;

the total inductance is, nevertheless, reasonably accurate). The cavity volume is V , its quality factor is Q , the eigenfrequencies of the perfectly conducting cavity are ω_n , ϵ_0 is the electric permittivity of free space, and the Coulomb gauge eigenfunctions have normalization

$$\frac{1}{V} \int_V \underline{A}_n \cdot \underline{A}_m dV = \delta_{nm}. \quad (8)$$

III. STATISTICS OF CAVITY FIELD

This paper is concerned with electrically large, complex cavities, for which a statistical description of the modes in (1) becomes applicable [7], [8], [9], [10], [11]. The cavity eigenvalues (resonant frequencies) ω_n have spacings that can be described by a slowly varying mean $\langle \Delta\omega_n \rangle$ times a random variable s

$$\Delta\omega_n = \omega_{n+1} - \omega_n = \langle \Delta\omega_n \rangle s \quad (9)$$

where the asymptotic formula for the mean is [12], [13]

$$\langle \Delta\omega_n \rangle \sim \pi^2 c^3 / (V \omega_n^2), \quad \omega_n \rightarrow \infty. \quad (10)$$

The probability density function for the normalized spacing s is Poisson (exponential) when the cavity geometry is simple (e.g., separable where eigenvalue degeneracy occurs frequently) [11], [12]

$$f_s^P(s) = e^{-s}, \quad 0 < s < \infty \quad (11)$$

and is Rayleigh (Wigner) when the cavity is complex [10], [12]

$$f_s^W(s) = \frac{\pi}{2} s e^{-s^2 \pi/4}, \quad 0 < s < \infty. \quad (12)$$

Complex geometry is typical of electromagnetic compatibility applications and thus the Rayleigh spacing is more frequently encountered. Constant spacing

$$s \equiv 1 \quad (13)$$

is also useful to study because, as will be shown later, it gives similar results for the impedance as does the Rayleigh spacing, and is simple enough that asymptotic analysis of the modal series (1) can be carried out.

The cavity eigenfunctions are taken to be isotropic (all three components have similar statistics) with Gaussian density [7], [11]

$$\zeta = \sqrt{3} A_{nz} \quad (14)$$

$$f_\zeta(\zeta) = \frac{1}{\sqrt{2\pi}} e^{-\zeta^2/2} \quad (15)$$

which follows the chosen normalization [7]

$$3 \int_{-\infty}^{\infty} A_{nz}^2 f_{A_{nz}}(A_{nz}) dA_{nz} = \int_{-\infty}^{\infty} \zeta^2 f_\zeta(\zeta) d\zeta = 1. \quad (16)$$

The normalization is assumed to be the same throughout the cavity. An argument in support of the Gaussian nature of the eigenfunctions relates to a ray description of these eigenfunctions, where the ray contributions to the modal field at an observation point consist of many separate returns from the complex cavity boundary that are uncorrelated [11], [7]. Experiments on cavities with smooth walls have shown that deviations from this

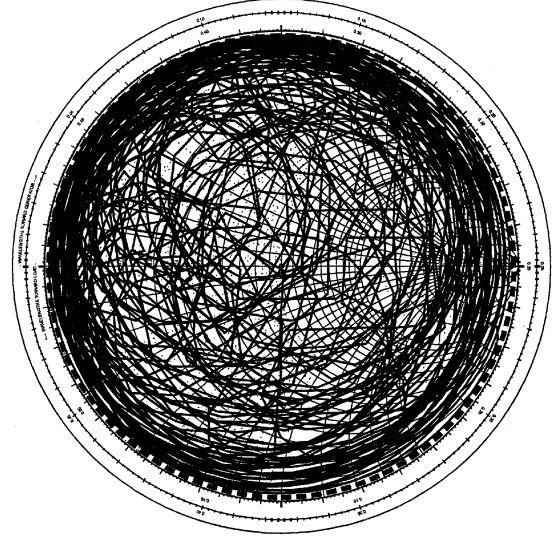


Fig. 1. Fifty-ohm Smith chart for input impedance of monopole at 220 MHz ($\alpha \approx 0.0609$) with 10-MHz sweep and 4800 uniformly spaced frequency points. “Bounding” power balance result comparison. Time dependence on the experimental Smith charts is $e^{j\omega t}$.

simple density do arise and can be included as contributions corresponding to periodic ray trajectories [11], [14], [15].

The correlation function for the eigenfunction components is different from that for scalar wavefunctions [11] and is given by [2], [16]

$$\begin{aligned} \rho_z(z_1, z_2) &= \frac{\langle A_{nz}(z_1) A_{nz}(z_2) \rangle}{\sqrt{\langle A_{nz}^2(z_1) \rangle \langle A_{nz}^2(z_2) \rangle}} \\ &\sim \frac{3}{2} \left(1 + \frac{1}{k_n^2} \frac{\partial^2}{\partial z_1^2} \right) \frac{\sin[k_n(z_1 - z_2)]}{k_n(z_1 - z_2)} \end{aligned} \quad (17)$$

where $k_n = \omega_n/c$ and the asymptotic symbol indicates the high order modes.

IV. EXPERIMENTS AND SIMULATIONS

The parameter that describes the degree of spectral overlap is

$$\alpha = k^3 V / (2\pi Q). \quad (18)$$

This parameter is the ratio of the energy stored in the cavity modes over a narrow spectral bandwidth (containing many complete modes) to the same energy if the field amplitude is fixed at the average peak level; it can be thought of as the ratio of modal width to modal spacing. If the cavity is undermoded (separate discrete modal spectra) $\alpha \ll 1$. If the cavity is overmoded (many overlapping modes) $\alpha \gg 1$. Figs. 1–3 show Smith charts for the measured input impedance of near resonant monopoles in the wall of a mode stirred chamber for the undermoded through overmoded range. The large variation of the input impedance exhibited over a relatively narrow frequency band is motivation for a statistical treatment. Thus the data for the input resistance shown in these figures will be reorganized into an ordered distribution in all future figures.

The mode stirred chamber (37 ft \times 23 ft \times 13 ft) has a volume of $V \approx 313 \text{ m}^3$. The cavity is not simply a rectangular box, since a mode stirrer was present in the chamber, but was not moved during the frequency sweeps that generated the data.

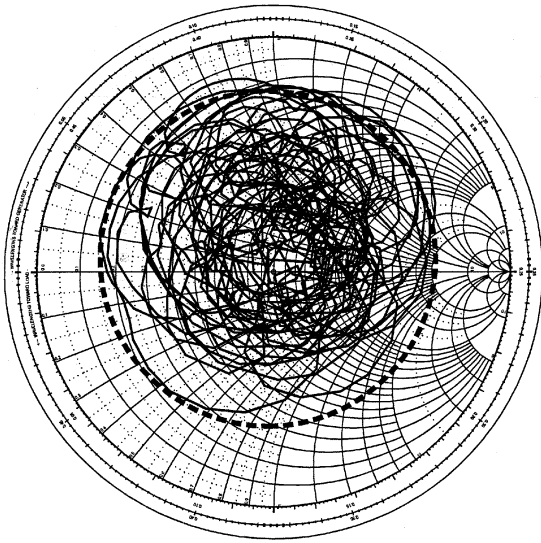


Fig. 2. Fifty-ohm Smith chart of input impedance of monopole at 920 MHz ($\alpha \approx 2.16$) with 1 MHz sweep and 801 uniformly spaced frequency points. "Bounding" power balance result comparison.

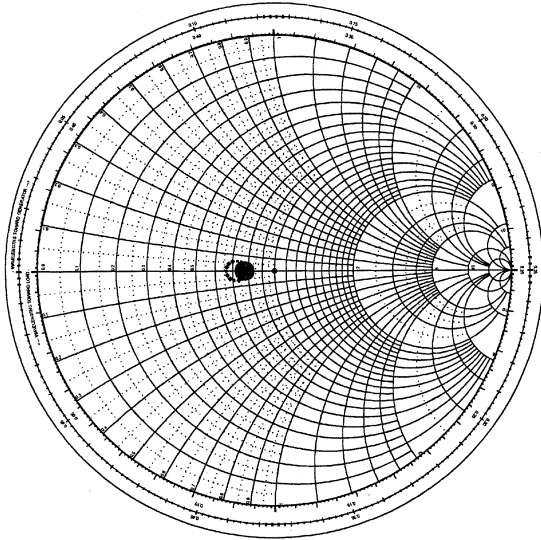


Fig. 3. Fifty-ohm Smith chart of input impedance of monopole at 15 GHz ($\alpha \approx 1206.7$) with 10 MHz sweep and 801 uniformly spaced frequency points. "Bounding" power balance result comparison.

The mode stirrer breaks degeneracy and makes Rayleigh statistics more applicable and slightly lowers the quality factor at the lower frequencies (rotation of the stirrer would span fewer resonant modes than the frequency sweeps at 220 MHz because of its limited size). The quality factor of the chamber was determined to have a mean value $Q \approx 80\,000$ by examining the 3 dB width of isolated modes at 220 MHz (the transmit and receive monopoles for this measurement, $h \approx 6.668$ cm and $h \approx 3.493$ cm, respectively, with $2a \approx 2.591$ mm, were taken as short as possible to minimize absorption, while maintaining sufficient signal-to-noise ratio); at 920 MHz it was estimated from the 220 MHz value, by the scaling $\sqrt{\omega}$, to be approximately $Q \approx 165\,000$; at 15 GHz it was taken as the experimental value (determined by measuring the mean field along with the net power into the chamber) 1 280 000. The mean quality factor at 220 MHz is significantly below the theoretical value $Q \sim$

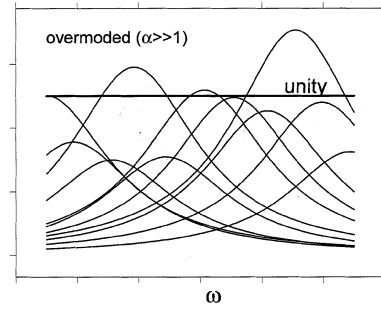


Fig. 4. Example of energy spectra when the cavity is overmoded $\alpha \gg 1$.

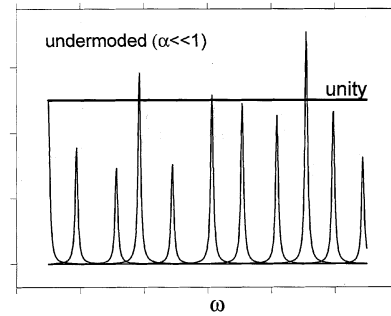


Fig. 5. Example of energy spectra when the cavity is undermoded $\alpha \ll 1$.

$3Vk\eta_0/(4SR_s) \approx 233\,000$, where $S \approx 303$ m² is the wall surface area and $R_s = 1/(\sigma\delta)$ is the surface resistance of the walls (where the skin depth is $\delta = \sqrt{2/(\omega\mu\sigma)}$, $\mu = \mu_0 = 4\pi \times 10^{-7}$ H/m and $\sigma \approx 2.6 \times 10^7$ S/m are the magnetic permeability and electrical conductivity of the walls, respectively). A small part of this reduction results from the roughness of the walls and the presence of the stirrer. However, because the variation about the mean is also larger than would be expected in a rectangular cavity with finitely conducting walls, it is thought that other loss mechanisms are present in the chamber.

The antennas were near-resonant wall-mounted monopoles. The dimensions of the monopoles were $2a \approx 2.591$ mm, $h \approx 32.90$ cm at 220 MHz, $h \approx 7.544$ cm at 920 MHz, and $2a \approx 1.51$ mm with $h \approx 4.325$ mm at 15 GHz.

Figs. 4 and 5 illustrate the behavior of the spectra for the two limits of α . Figs. 6 and 7 show comparisons of the monopole input resistance with Monte Carlo simulation of the series

$$z_{\text{in}} = r_{\text{in}} - ix_{\text{in}} = (Z_{\text{in}} - Z)/R_{\text{rad}} \\ \approx \left(\frac{2\pi Q}{k^3 V} \right) \sum_{n_r} \frac{i\omega/(2Q)}{\omega(1 + i/(2Q)) - \omega_n} 3A_{nz}^2(\underline{r}) \quad (19)$$

where we have approximated the summand (Q and $\langle \Delta\omega_n \rangle$ are approximated as constant also) since we are including only those modes near the observation range of ω values captured in the figures (the range of included modes n_r contains a range of ω_n that is slightly larger than the observation ω range so that negligible error is incurred in this approximation). The simulations were done with all three types of eigenvalue spacings. The agreement with the experimental results is good; although there is some small variation with realization of the random numbers, the Rayleigh and uniform spacing results

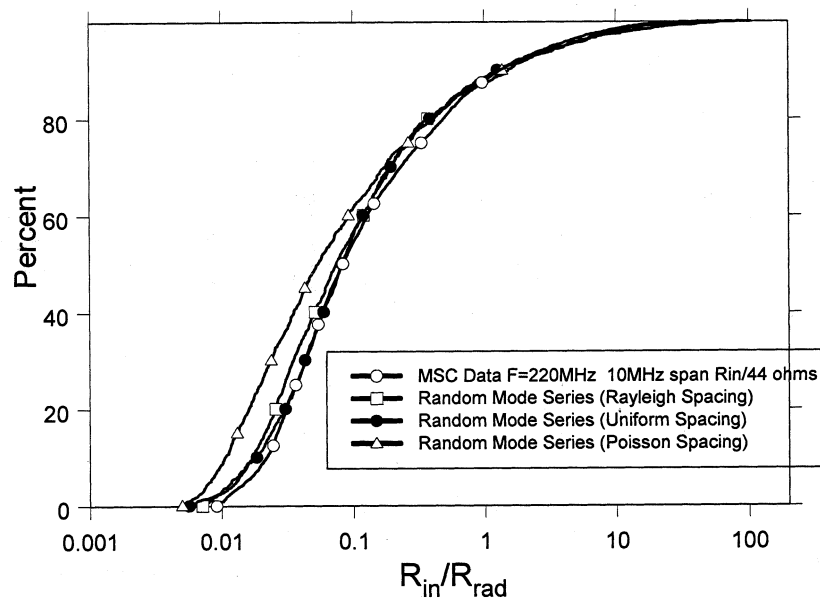


Fig. 6. Normalized input resistance distribution from simulations and experiment at 220 MHz ($\alpha \approx 0.0609$).

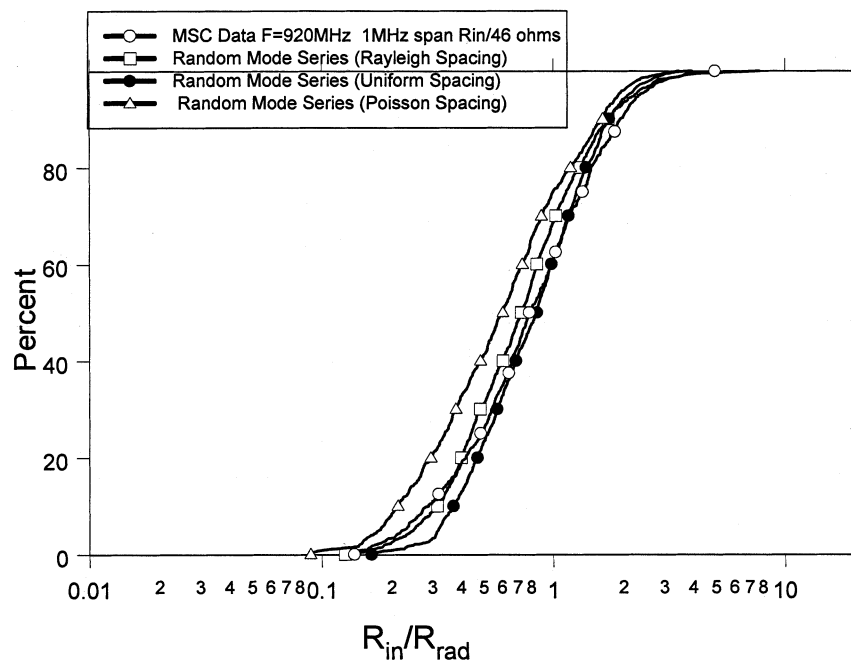


Fig. 7. Normalized input resistance distribution from simulations and experiment at 920 MHz ($\alpha \approx 2.16$).

are in slightly better agreement with measurements than the Poisson spacing.

The near resonant monopoles in the experiment had nearly zero free space reactance (except the 920 MHz antenna which had the experimentally determined value $j8.5$ ohms, $e^{j\omega t}$ time dependence is used in the Smith chart figures). The experimentally determined free space value of the radiation resistances were 44 ohms at 220 MHz and 46 ohms at 920 MHz. These experimental values of radiation resistance are slightly above the values expected for such antennas but were nevertheless used to normalize the cavity impedance data. The frequency span was

10 MHz with 4800 frequency points in the 220 MHz experiment; the simulations used 200 modes with 1000 frequency points. The frequency span was 1 MHz with 801 frequency points in the 920 MHz experiment; the simulations used 400 modes with 1000 frequency points. The frequency span was 10 MHz also with 801 frequency points in the 15 GHz experiment.

V. ASYMPTOTIC BEHAVIORS

Using the modal series (1) it can be shown that the frequency average [taken over a narrow band, but including many complete

modal spectra with mean spacing $\langle \Delta\omega \rangle = \pi^2 c^3 / (V\omega^2)$ of the normalized input impedance is nearly unity [1]

$$\langle z_{\text{in}} \rangle_{\omega} = \frac{1}{\omega_+ - \omega_-} \int_{\omega_-}^{\omega_+} z_{\text{in}} d\omega \rightarrow 1$$

$$\langle \Delta\omega \rangle \ll \omega_+ - \omega_- \ll \omega. \quad (20)$$

It can also be shown in the overmoded limit that by replacing the modal sum by an integral (inserting $d\omega_n / \langle \Delta\omega_n \rangle$ in the summand) the normalized impedance approaches unity [1]

$$z_{\text{in}} \rightarrow 1, \quad \alpha \rightarrow \infty. \quad (21)$$

In the next two subsections the uniformly spaced modal series is used to estimate the behaviors of the extreme values of the impedance. The final subsection estimates the variance in the overmoded limit.

A. Uniform Spacing, Single Mode

The undermoded limit $\alpha \ll 1$ has separated, discrete, spectra. The largest values of the input resistance and reactance in this region occur when ω is near a resonance. Thus we can consider a single mode of the series (the mode closest to the observation frequency) and estimate the extreme statistics by regarding $\omega - \omega_n$ to be a random variable with uniform density between $\pm \langle \Delta\omega_n \rangle / 2$ (for typically used uniform frequency sampling). The distribution function, derived from the ratio of independent random variables [17] (ratio of Gaussian squared to shifted uniform squared random variables), for this case is [1]

$$F(r_{\text{in}}) = 1 - \int_{r_{\text{in}}}^{\infty} f(r) dr \sim 1 + \frac{\alpha}{\pi} \sqrt{r_{\text{in}}\alpha / (2\pi)} e^{-r_{\text{in}}\alpha/4}$$

$$\cdot [K_0(r_{\text{in}}\alpha/4) - K_1(r_{\text{in}}\alpha/4)], \quad r_{\text{in}} \gg \alpha, \alpha \ll 1 \quad (22)$$

where the identity [18] $\int_0^{\infty} e^{-\nu x} (dx / \sqrt{x(x+a)}) = e^{\nu a/2} K_0(\nu a/2)$ has been used and $K_0(x)$, $K_1(x)$ are the modified Bessel functions. Figs. 8 and 9 show this result (long dashed curves) compared to measurements and Monte Carlo simulations of (19) with uniform spectral spacing (α is too large in Fig. 9 for this result to be valid over any substantial range of r_{in}). Over most of the valid range (22) can be simplified to

$$F(r_{\text{in}}) \approx 1 - \frac{2}{\pi} \sqrt{\frac{2\alpha}{\pi r_{\text{in}}}}, \quad 1/\alpha \gg r_{\text{in}} \gg \alpha. \quad (23)$$

However, near the upper limit of r_{in} , the corresponding density function exhibits exponential behavior that allows one to establish practical upper bounds for the resistance values

$$f(r_{\text{in}}) \approx \frac{e^{-r_{\text{in}}\alpha/2}}{\pi r_{\text{in}}} \alpha, \quad r_{\text{in}}\alpha \gg 1. \quad (24)$$

The normalized reactance also exhibits exponential behavior near the upper limit (an averaging method [19] can be used to give a more uniformly valid expression) [1]

$$f(x_{\text{in}}) \approx \frac{\alpha\sqrt{2}}{\pi |x_{\text{in}}|} e^{-|x_{\text{in}}|\alpha}, \quad |x_{\text{in}}|\alpha \gg 1 \quad (25)$$

which shows that the extreme reactance magnitude is approximately half the extreme resistance.

The number of independent samples in a frequency sweep is dependent on the number of modes spanned. For example at

220 MHz there are only 141 modes in the frequency sweep even though there are many more frequencies sampled. If, for $\alpha \ll 1$, the frequency sweep is sufficiently fine to resolve the spectral peaks (over-sampling in frequency) then the density function of the peaks is of interest. Thus, near the upper limit of r_{in} we can set $\omega = \omega_n$ and find the single mode density function for the peak values (the square of a Gaussian random variable)

$$f(r_{\text{in}}) \approx \sqrt{\frac{\alpha}{2\pi r_{\text{in}}}} e^{-r_{\text{in}}\alpha/2}, \quad r_{\text{in}}\alpha \gg 1. \quad (26)$$

The exponential behavior in (26) is the same as (24). The distribution function for the peak values corresponding to (26) is

$$F(r_{\text{in}}) \approx \text{erf}\left(\sqrt{r_{\text{in}}\alpha/2}\right) \quad (27)$$

where $\text{erf}(x)$ is the error function, and the number of independent samples corresponds to the number of modes contained in the frequency sweep.

B. Uniform Spacing, Between Modes

The smallest values of the input resistance for $\alpha \ll 1$ occur when ω is between modes. Taking the observation frequency ω to be exactly between modes of the series (19) with uniform spectral spacing, the modal terms can be taken in pairs about the observation frequency, each pair having a simple exponential distribution. The infinite summation requires an infinite sequence of convolutions to be performed to obtain the density function [17]. Using the Laplace transform to convert the convolutions to an infinite product, and using the identity [20]

$$\prod_{k=1}^{\infty} \left[1 - \frac{x^2}{k^2 - a^2} \right] = \frac{a}{\sqrt{a^2 + x^2}} \frac{\sin(\pi\sqrt{a^2 + x^2})}{\sin(\pi a)}$$

to evaluate the product, the density can be found by inverse transform of the resulting function for frequency samples between modes. The integral of the density function is thus the distribution [1]

$$F(r_{\text{in}}) = F_{\chi} \left(\frac{\pi^2 r_{\text{in}}}{8\alpha} \right) \quad (28)$$

where from the residue method

$$F_{\chi}(\chi) = 1 - e^{-\chi^2/4} \cosh(\chi) \frac{4}{\pi} \sum_{m=0}^{\infty} (-1)^m$$

$$\cdot \frac{2m+1}{(2m+1)^2 + 4\chi^2/\pi^2} e^{-(2m+1)^2\chi}. \quad (29)$$

An alternative representation for the density function $f_{\chi}(\chi)$, where $f(r_{\text{in}}) = f_{\chi}(\pi^2 r_{\text{in}} / (8\alpha)) \pi^2 / (8\alpha)$, that converges rapidly for $\chi \rightarrow 0$, can also be obtained from the inverse transform using the identity [21]

$$\frac{a}{2\sqrt{\pi t^3}} e^{-a^2/(4t)} = \frac{1}{2\pi i} \int_{c-i\infty}^{c+i\infty} e^{st} e^{-a\sqrt{s}} ds$$

(although it is difficult to integrate to obtain the distribution function) [1]

$$f_{\chi}(\chi) = e^{-\chi^2/4} \cosh(\chi) \sqrt{\frac{\pi}{\chi^3}} \sum_{m=0}^{\infty} (-1)^m (m+1/2)$$

$$\cdot e^{-(m+1/2)^2\pi^2/(4\chi)}. \quad (30)$$

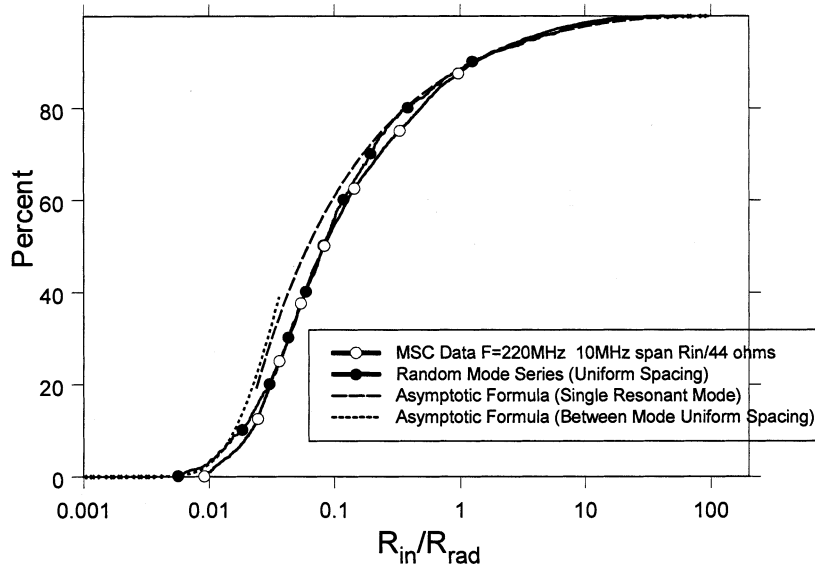


Fig. 8. Comparison of asymptotic formulas, simulation, and experiment at 220 MHz with 10-MHz sweep.

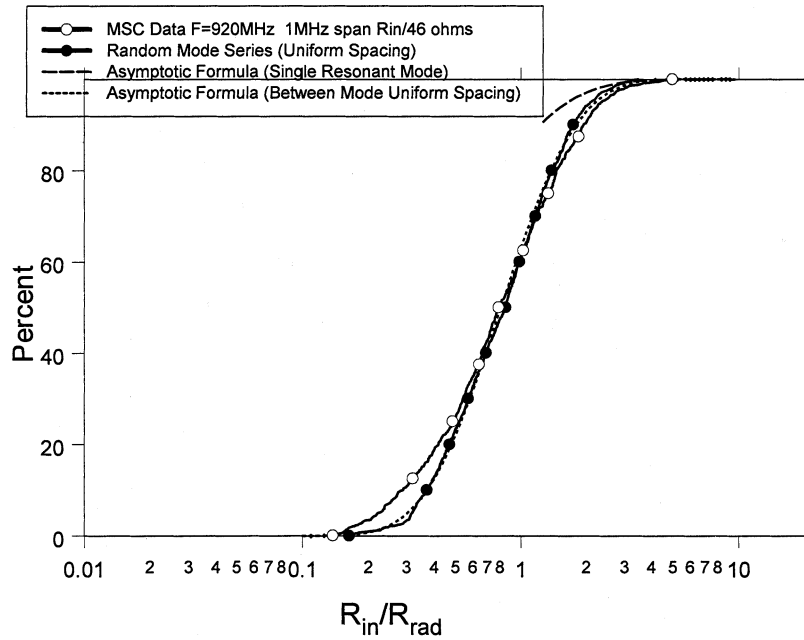


Fig. 9. Comparison of asymptotic formulas, simulation, and experiment at 920 MHz with 1-MHz sweep.

Figs. 8 and 9 show the distribution function (28) (short dashed curves) compared to measurements and Monte Carlo simulations (this result describes the entire distribution in Fig. 9 since the placement of the observation frequency ω is not critical when the modes are overlapping and α is of order unity).

Using the second representation (30) we see that the density function exhibits exponential decay for very small r_{in}

$$f(r_{in}) \sim \cosh(\alpha) \sqrt{\frac{2\alpha}{\pi r_{in}^3}} e^{-\alpha(r_{in}+1/r_{in})/2}, \quad r_{in} \ll \alpha \quad (31)$$

which again allows one to establish practical lower bounds for the input resistance. For $\alpha \ll 1$, the $\alpha r_{in}/2$ term in the exponen-

tial can be dropped, and (31) can be integrated to give the distribution function $F(r_{in}) \approx 2\text{erfc}[\sqrt{\alpha/(2r_{in})}]$, where $\text{erfc}(x)$ is the complementary error function. The number of independent samples, when we are over-sampling in frequency, is again the number of modes spanned in the frequency sweep.

For α of order unity, the first representation (29) can be used to give

$$f(r_{in}) \sim \frac{\pi}{2\alpha} \cosh(\alpha) e^{-r_{in}[(2\alpha)/\pi + \pi/(2\alpha)]\pi/4}, \quad r_{in} \rightarrow \infty, \quad \alpha = O(1) \quad (32)$$

showing the exponential decay for large r_{in} . If we take the over-moded limit $\alpha \gg 1$, from the second representation (31) we

find that the normalized input resistance is Gaussian distributed about the mean of unity

$$f(\rho_r) \sim \sqrt{\frac{\alpha}{2\pi}} e^{-\alpha \rho_r^2/2}, \quad r_{\text{in}} = 1 + \rho_r, \quad \alpha \rightarrow \infty. \quad (33)$$

C. Overmoded Limit

By the central limit theorem [17] we expect both components of the impedance to become Gaussian distributed in the overmoded limit $\alpha \gg 1$ since many modes are equally contributing to the modal series. Finding the variance of both components thus allows us to write

$$z_{\text{in}} \sim 1 + r_0 \zeta - i x_0 \zeta', \quad \alpha \gg 1 \quad (34)$$

where ζ and ζ' are independent, normalized, zero mean Gaussians, and the standard deviations are found to be [1]

$$r_0 = x_0 = 1/\sqrt{\alpha}. \quad (35)$$

VI. ELECTRICALLY LONGER ANTENNA

The preceding analytical and simulation results were based on the assumption of an electrically short dipole, but the experiments were conducted using near resonant monopole antennas. This conflicting situation will be resolved in the present and next sections. Using the representations from the Appendix (69), (74), (75), and (77), the integro-differential equation for a center driven linear antenna (with drive voltage V_0) inside a cavity can be written as

$$\begin{aligned} -V_0 \delta(z) &= E_z \\ &\approx -\frac{i\omega}{\epsilon_0 V} \sum_n \frac{\omega^2/\omega_n^2}{\omega^2(1+i/Q) - \omega_n^2} A_{\text{nz}}(z) \\ &\quad \cdot \int_{-h}^h A_{\text{nz}}(z') I(z') dz' + \frac{i\omega\mu_0}{4\pi} \\ &\quad \cdot \left[\left(1 + \frac{1}{k^2} \frac{\partial^2}{\partial z^2} \right) \int_{-h}^h \frac{I(z') dz'}{\sqrt{a^2 + (z - z')^2}} - I(z) \right] \end{aligned} \quad (36)$$

where the second term is the local quasistatic contribution. The antenna current distribution $I(z)$ is the unknown. The antenna is assumed to be thin and thus the local quasistatic term can be thought of as approaching the transmission line form [22], [23]

$$\begin{aligned} \left(1 + \frac{1}{k^2} \frac{\partial^2}{\partial z^2} \right) \int_{-h}^h \frac{I(z') dz'}{\sqrt{a^2 + (z - z')^2}} \\ \approx \Omega_e \left(1 + \frac{1}{k^2} \frac{\partial^2}{\partial z^2} \right) I(z). \end{aligned} \quad (37)$$

This term, in addition to the boundary conditions

$$I(\pm h) = 0 \quad (38)$$

play a dominant role in determining the distribution of current (at least up to the first resonance). By means of (37) and (38), the leading term of the current can thus be taken as the usual sinusoid

$$I(z) \approx I_0 \sin k(h - |z|). \quad (39)$$

More accurate approximations could be constructed by the addition of random components to the distribution. The impedance is then found by using this current, and the integro-differential representation for the electric field (36), in the stationary (first order corrections to the current do not contribute) EMF representation (78) [6]

$$Z_{\text{in}} = -\frac{1}{I^2(0)} \int_{-h}^h E_z(z) I(z) dz. \quad (40)$$

Noting that the integral of a Gaussian random process is a Gaussian random variable [17] we find

$$\begin{aligned} Z_{\text{in}} \approx R - iX + \sum_n \left(\frac{\eta_0 k^2}{2\pi} U_n^{\text{tot}} \right) \left(\frac{2\pi Q}{k^3 V} \right) \\ \cdot \frac{(i\omega^2/Q) \omega^2/\omega_n^2}{\omega^2(1+i/Q) - \omega_n^2} 3A_{\text{nz}}^2 \end{aligned} \quad (41)$$

where again the antenna ohmic resistance is R and the local reactance is (we are ignoring quasistatic images in the cavity walls)

$$\begin{aligned} X \approx -\frac{\eta_0}{2\pi} \Omega_e \cot(kh) + \frac{\eta_0}{2\pi} \frac{1}{\sin^2(kh)} \\ \cdot [2\text{Si}(kh) + \sin(2kh) \{2\text{Cin}(kh) - \text{Cin}(2kh) - \frac{3}{4}\} \\ - \cos(2kh) \{\text{Si}(2kh) - 2\text{Si}(kh)\} - \frac{1}{2}kh] \end{aligned} \quad (42)$$

and $\text{Si}(x)$, $\text{Cin}(x)$ are the sine and cosine integrals. The local reactance (42) is simply the contribution of the local quasistatic term (second term) in (36) to the impedance in (40). The quantity U_n^{tot} in (41) is the variance of the stochastic integral appearing in the impedance representation (40) and is given by

$$\begin{aligned} U_n^{\text{tot}} = \frac{1}{\sin^2(kh)} \int_{-h}^h \sin k(h - |z|) \int_{-h}^h \frac{3}{2} \left(1 + \frac{1}{k_n^2} \frac{\partial^2}{\partial z^2} \right) \\ \cdot \frac{\sin k_n(z - z')}{k_n(z - z')} \sin k(h - |z'|) dz' dz. \end{aligned} \quad (43)$$

A small error is made (mostly in the reactance) if we set $k_n \rightarrow k$ in U_n^{tot} for all values of α [this approximation is consistent with the previously discussed truncation of the series (19) in the range of the resonant modes]. Note that, if k_n is retained in U_n^{tot} , it can be shown [1] in the overmoded limit $\alpha \gg 1$, then the correct total antenna reactance [6]

$$\begin{aligned} X_{\text{in}} = -\frac{\eta_0}{2\pi} \Omega_e \cot(kh) + \frac{\eta_0}{4\pi} \\ \cdot [2\text{Si}(2kh) + \sin(2kh) \{-2 + 2\text{Cin}(2kh) - \text{Cin}(4kh)\} \\ - \cos(2kh) \{\text{Si}(4kh) - 2\text{Si}(2kh)\}] / \sin^2(kh) \end{aligned}$$

is produced rather than the value X , that is obtained when the approximation $k_n \rightarrow k$ is invoked; at low frequencies $kh \ll 1$, X and X_{in} become the same; even for $kh = \pi/2$, where the dominant leading term of the reactance vanishes, the error is $X \approx 64$ ohms versus the correct $X_{\text{in}} \approx 43$ ohms. It is recognized that the right hand side of (43), with $k_n \rightarrow k$, is just $R_{\text{rad}} 2\pi / (\eta_0 k^2)$, where R_{rad} is the free space radiation resistance of the electrically longer antenna [6]

$$\begin{aligned} (4\pi/\eta_0) \sin^2(kh) R_{\text{rad}} \\ = 2\text{Cin}(2kh) + \sin 2kh [\text{Si}(4kh) - 2\text{Si}(2kh)] \\ - \cos 2kh [\text{Cin}(4kh) - 2\text{Cin}(2kh)]. \end{aligned} \quad (44)$$

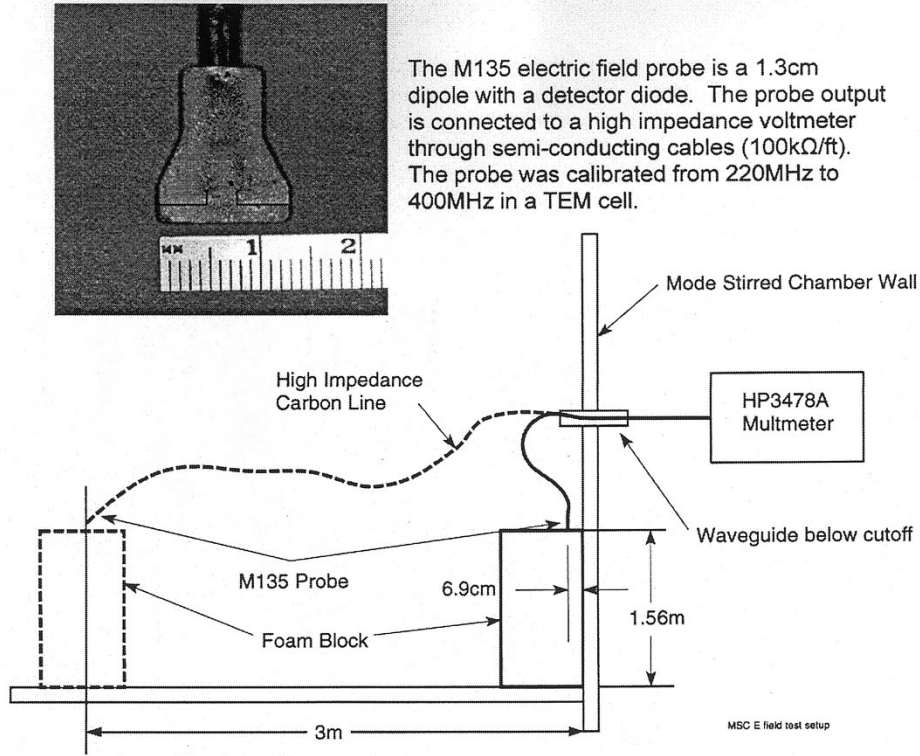


Fig. 10. Drawing of 3 dB wall enhancement field measurement at 220 MHz using dipole probe.

Therefore, using this simplification in (41), we find

$$Z_{\text{in}} \approx R - iX + R_{\text{rad}} \sum_n \left(\frac{2\pi Q}{k^3 V} \right) \frac{(i\omega^2/Q)\omega^2/\omega_n^2}{\omega^2(1+i/Q) - \omega_n^2} 3A_{nz}^2. \quad (45)$$

Surprisingly, this is the same form we had previously for the short antenna, except that the radiation resistance R_{rad} is now the correct free space value for the electrically longer antenna. Thus the quantity $z_{\text{in}} = (Z_{\text{in}} - Z)/R_{\text{rad}}$ from the electrically short antenna theory given before is approximately the same for electrically longer antennas.

VII. MONOPOLE ANTENNA AND WALL BEHAVIOR

A previous paper [16] has shown that the correlation dyad for the field is proportional to the imaginary part of the dyadic Green's function. Thus in a local vicinity of the cavity boundary (near the wall mounted monopole antenna) at $z = 0$, we can use the half space dyadic Green's function to obtain the correlation function transition near the cavity wall. The result is

$$R_{zz}^h(z_1, z_2) = \frac{\langle A_{nz}(z_1) A_{nz}(z_2) \rangle}{\sqrt{\langle A_{nz}^2(z_1) \rangle \langle A_{nz}^2(z_2) \rangle}} \sim \frac{3}{2} \left(1 + \frac{1}{k_n^2} \frac{\partial^2}{\partial z_1^2} \right) \cdot \left[\frac{\sin k_n(z_1 - z_2)}{k_n(z_1 - z_2)} + \frac{\sin k_n(z_1 + z_2)}{k_n(z_1 + z_2)} \right]. \quad (46)$$

Using this correlation function, it is easy to show [1] that the impedance of a wall-mounted monopole is half that of the dipole. Thus, again the quantity $z_{\text{in}} = (Z_{\text{in}} - Z)/R_{\text{rad}}$ for the monopole is the same as for the dipole (assuming R_{rad} is taken

to be the monopole free space radiation resistance), and the comparisons with experiment, made above, are justified.

It is interesting that the known 3 dB wall enhancement of the normal electric field [24], and its transition into the cavity volume are represented by this half space correlation function

$$\frac{\langle |E_{\text{norm}}|^2 \rangle}{\langle |E_i|^2 \rangle} = R_{zz}^h(z, z) \sim 1 + \frac{3}{2} \left(1 + \frac{\partial^2}{\partial u^2} \right) \frac{\sin u}{u} \Big|_{u=2kz}. \quad (47)$$

Figs. 10–12 show a mode stirred chamber experiment and results verifying the presence of this wall enhancement in the undermoded region. The normal electric field distribution on the wall is 3 dB higher than in the volume of the cavity (this is borne out for the field as a function of frequency in Fig. 11, and approximately for the field at the resonant mode frequencies in Fig. 12). The frequency range included in these figures is from 220–230 MHz (6381 points are included in the close spacing in Fig. 11 and 5561 points are included in the far spacing in Fig. 11).

VIII. POWER BALANCE

Now that the usefulness of the electrically short antenna theory has been demonstrated, we return to the electrically short antenna and develop a simple engineering model.

We break up the field E_z at the antenna into the sum of a reflected part E_z^{ref} and a part E_z^{rad} radiated as if in free space. The impedance components of the short dipole are correspondingly broken into the sums

$$R_{\text{in}} = R_{\text{rad}} + R_{\text{wall}} \quad (48)$$

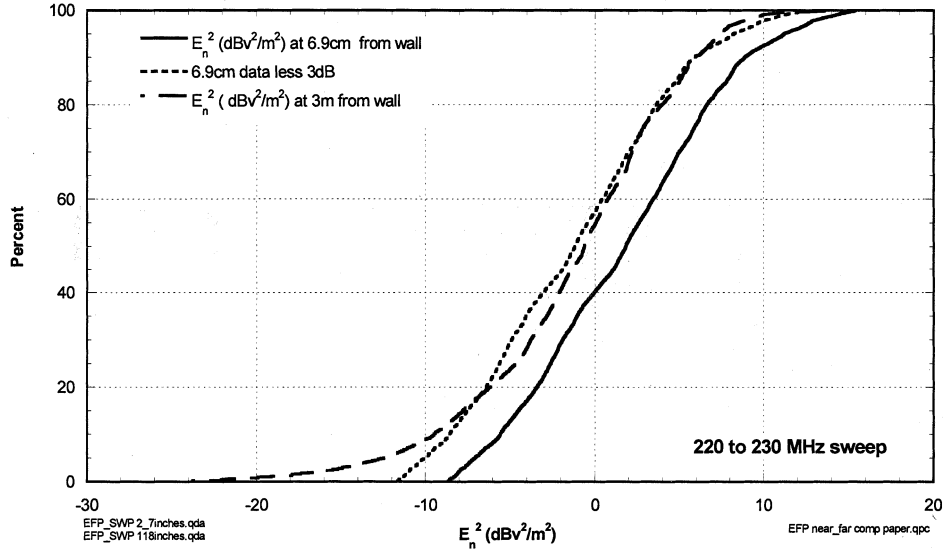


Fig. 11. Electric field distribution from two dipole probes, one 6.9 cm from wall and one 3 m from wall, showing 3 dB wall enhancement.

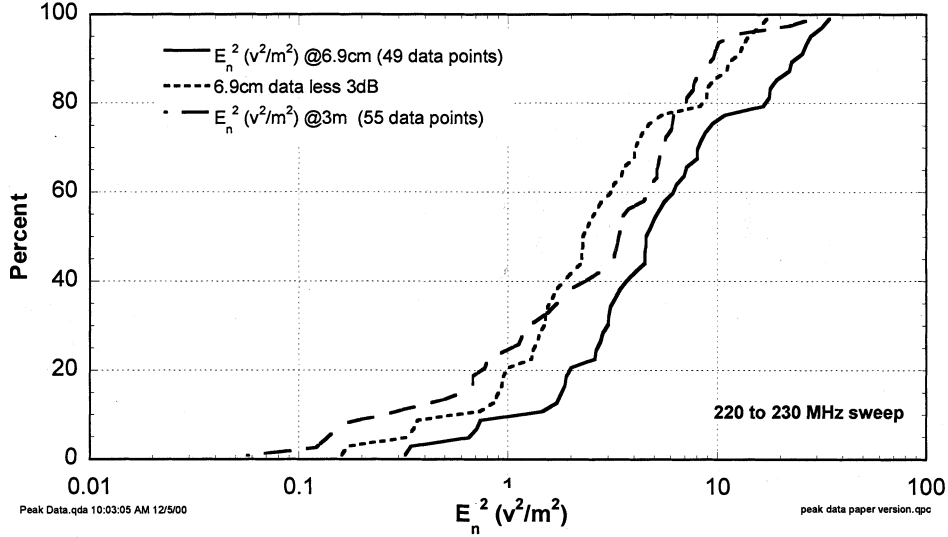


Fig. 12. Electric field distribution from resonance peaks for both probes showing 3 dB wall enhancement.

and

$$X_{in} = X + X_{wall}. \quad (49)$$

The quantity R_{rad} is the free space radiation resistance associated with the field E_z^{rad} and X is the local reactance associated with the quasistatic part of the field E_z^{rad} . The quantities R_{wall} and X_{wall} are associated with the reflected field from the cavity wall E_z^{ref} . The wall impedance $Z_{wall} = R_{wall} - iX_{wall}$ can be written in terms of the received voltage at the dipole due to the reflected field $V_{ref} \sim -hE_z^{ref}$. Thus

$$Z_{wall} = V_{ref}/I(0) = -hE_z^{ref}/I(0) = \frac{-E_z^{ref}}{\sqrt{\langle |E_z|^2 \rangle_V}} h \sqrt{U / (|I(0)|^2 3\epsilon_0/2)} \quad (50)$$

where the received voltage has been determined from the effective height (the positive reference of the voltage is on the positive

z arm of the antenna) of the short dipole, and the mean energy density in the cavity is

$$U = \frac{3}{2} \epsilon_0 \langle |E_z|^2 \rangle_V \quad (51)$$

where the subscript V denotes volume average. Now using the definition of cavity quality factor

$$Q = \frac{\omega V U}{P_{in}} \quad (52)$$

with the average power into the antenna (the dissipated power) given by

$$P_{in} = \frac{1}{2} R_{in} |I(0)|^2 \quad (53)$$

we obtain

$$Z_{wall} = \frac{-E_z^{ref}}{\sqrt{\langle |E_z|^2 \rangle_V}} \sqrt{\frac{Q h^2 R_{in} \eta_0}{3kV}}. \quad (54)$$

Introducing R_{rad} , given in (2), and α , given by (18), into (54), and using lower case impedances to denote the quantities $r_{\text{wall}} = R_{\text{wall}}/R_{\text{rad}}$ and $x_{\text{wall}} = X_{\text{wall}}/R_{\text{rad}}$ (note that this scaled reactance is really the same as x_{in} , since x_{in} was defined with the local reactance subtracted out), we finally obtain

$$r_{\text{wall}} = r_{\text{in}} - 1 = \tau \sqrt{r_{\text{in}}/\alpha} \quad (55)$$

$$x_{\text{wall}} = \zeta \sqrt{r_{\text{in}}/\alpha} \quad (56)$$

where

$$\tau = \frac{-\text{Re}(E_z^{\text{ref}})}{\sqrt{\langle |E_z|^2 \rangle_V}} \quad (57)$$

$$\zeta = \frac{\text{Im}(E_z^{\text{ref}})}{\sqrt{\langle |E_z|^2 \rangle_V}}. \quad (58)$$

A. Extreme Values

The quantities τ and ζ in (55) and (56) describe the fluctuation of the real and imaginary parts of the reflected field at the antenna location normalized by the mean cavity field. For the present we assume τ and ζ have normalized Gaussian densities with zero mean (this assumption is refined in the next subsection). To obtain an extreme value curve for the impedance variation we could take these random variables to be fixed at, say, the three sigma point $M_0 = 3$ of the underlying real and imaginary Gaussian distributions. It is interesting to note that if the cavity field is viewed as a three dimensional standing wave in the frequency range of the fundamental cavity modes, then the maximum-to-mean-ratio of the field is 8:1, corresponding to the value $M_0 = 2\sqrt{2}$; a value not very different from the three sigma value $M_0 = 3$; **these extreme results may therefore be useful at lower frequencies than anticipated.** Setting $\tau = M_0 \cos \varphi$ and $\zeta = M_0 \sin \varphi$ and solving the quadratic equation gives

$$r_{\text{in}} = 1 + \frac{1}{2\alpha} M_0^2 \cos^2 \varphi \pm \sqrt{\left(1 + \frac{1}{2\alpha} M_0^2 \cos^2 \varphi\right)^2 - 1} \quad (59)$$

$$x_{\text{wall}} = M_0 \sin \varphi \sqrt{r_{\text{in}}/\alpha} \quad (60)$$

where the \pm sign is chosen consistent with the sign of $\cos \varphi$. The dashed circles in Figs. 1–3 are plots of these results with $M_0 = 3$ (and φ ranging over values between $-\pi$ and π). These extreme circles provide a reasonable containment of the experimental impedance variations. The radiation resistance of the 15 GHz monopole was taken as the nominal 36 ohms value.

The extreme values of the real and imaginary parts on this circle can be easily found as

$$1 + \frac{1}{2\alpha} M_0^2 - \sqrt{\left(1 + \frac{1}{2\alpha} M_0^2\right)^2 - 1} < r_{\text{in}} < 1 + \frac{1}{2\alpha} M_0^2 + \sqrt{\left(1 + \frac{1}{2\alpha} M_0^2\right)^2 - 1} \quad (61)$$

$$|x_{\text{wall}}| < \sqrt{\left(1 + \frac{1}{2\alpha} M_0^2\right)^2 - 1}. \quad (62)$$

The highly undermoded limit is $1/(2 + M_0^2/\alpha) < r_{\text{in}} < (2 + M_0^2/\alpha)$ and $2|x_{\text{wall}}| < 2 + M_0^2/\alpha$. The highly overmoded limit is $1 - M_0/\sqrt{\alpha} < r_{\text{in}} < 1 + M_0/\sqrt{\alpha}$ and $|x_{\text{wall}}| < M_0/\sqrt{\alpha}$, thus giving $r_{\text{in}} \rightarrow 1$ and $x_{\text{wall}} \rightarrow 0$.

B. Density

The distribution of input resistance generated by the power balance results, with the normalized Gaussian assumption for the normalized reflected field in (55), is shown as the dotted curves in Figs. 13 and 14. The extreme values are reasonable but the midrange distribution is not even close to the experimental or simulation results. Using the modal series field representation for a short dipole in a cavity we can generate the actual distributions for τ and ζ in (57) and (58), from which we construct more accurate density function approximations. Using short dipole representations from the Appendix (80) and (83) in (82), along with (81) gives

$$\begin{aligned} \frac{-E_z^{\text{ref}}}{\sqrt{\langle |E_z|^2 \rangle_V}} &= i \frac{\sum_n \frac{3A_{nz}^2 \omega^2 / \omega_n^2}{|\omega^2(1+i/Q) - \omega_n^2|}}{\sqrt{\sum_n \frac{3A_{nz}^2}{|\omega^2(1+i/Q) - \omega_n^2|^2}}} \frac{I(0)}{|I(0)|} \\ &\quad - \alpha \frac{Q/\omega^2}{\sqrt{\sum_n \frac{3A_{nz}^2}{|\omega^2(1+i/Q) - \omega_n^2|^2}}} \frac{I(0)}{|I(0)|} \\ &\approx i \frac{\sum_{n_r} \frac{3A_{nz}^2}{\pi(\omega - \omega_n)/\langle \Delta\omega_n \rangle + i\alpha}}{\sqrt{\sum_{n_r} \frac{3A_{nz}^2}{|\pi(\omega - \omega_n)/\langle \Delta\omega_n \rangle + i\alpha|^2}}} \\ &\quad - \frac{1}{\sqrt{\sum_{n_r} \frac{3A_{nz}^2}{|\pi(\omega - \omega_n)/\langle \Delta\omega_n \rangle + i\alpha|^2}}} \end{aligned} \quad (63)$$

where $I(0)$ is taken to be real and positive (this choice is to be noted when interpreting the real and imaginary parts of the reflected field) and we have included only the resonant-range terms in the final approximation. The first term, which corresponds to the total normalized field at the antenna, has a positive real part. The second term, which corresponds to the normalized radiated field at the antenna, is negative real. Note that the local quasistatic normalized field has been subtracted from each term in the difference. In the undermoded limit $\alpha \ll 1$, the first term is imaginary except in the narrow frequency band about the resonances. The real part is thus skewed toward negative values. Thus we try taking the asymmetric Gaussian density

$$\begin{aligned} f(\tau) &\approx \frac{p(\alpha)}{\sqrt{2\pi}} e^{-\tau^2/2}, \quad 0 < \tau < \infty \\ &\approx \frac{2 - p(\alpha)}{\sqrt{2\pi}} e^{-\tau^2/2}, \quad -\infty < \tau < 0 \end{aligned} \quad (64)$$

as a fit to the density function of the real part of the normalized reflected field (63). If we apply the result from (20), that $\langle r_{\text{in}} \rangle_\omega = \langle r_{\text{in}} \rangle_\tau \rightarrow 1$, we can determine the function of α as

$$p(\alpha) = 1 - 1 / \left[2\sqrt{2\alpha/\pi} + e^{2\alpha} \text{erfc}(\sqrt{2\alpha}) \right]. \quad (65)$$

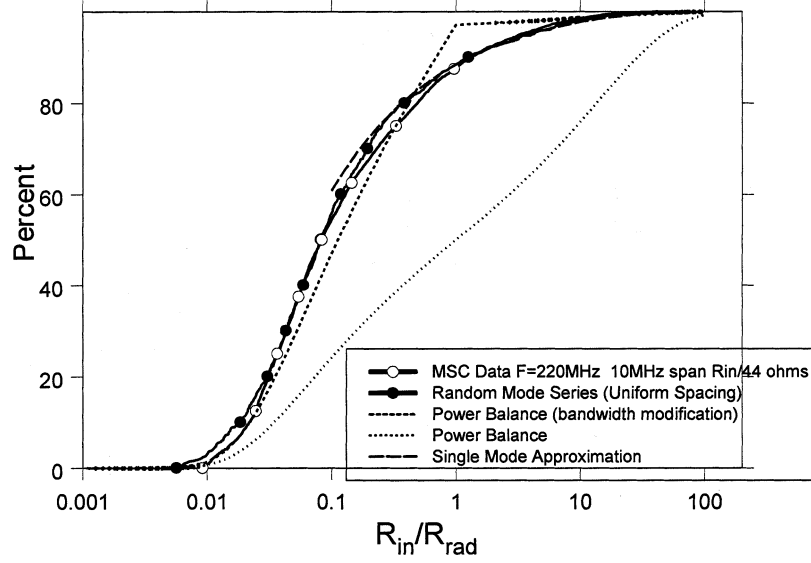


Fig. 13. Normalized input resistance distribution from simulation, power balance (the bandwidth modification curve uses the asymmetric Gaussian reflected field distribution) and experiment at 220 MHz.

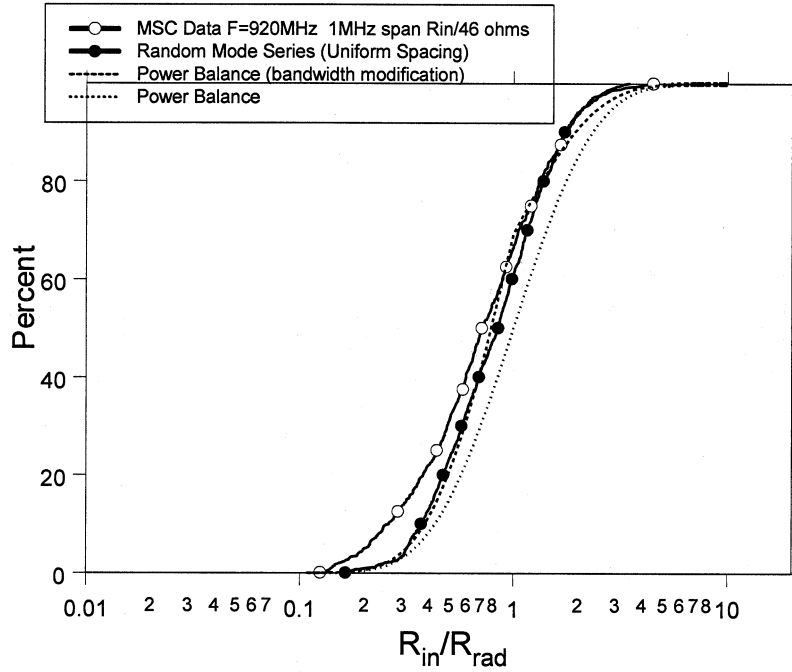


Fig. 14. Normalized input resistance distribution from simulation, power balance (the bandwidth modification curve uses the asymmetric Gaussian reflected field distribution) and experiment at 920 MHz.

The function $p(\alpha)$ approaches 2α as $\alpha \rightarrow 0$ and approaches 1 as $\alpha \rightarrow \infty$. Figs. 15 and 16 show a comparison of the distributions for the real and imaginary parts of the normalized reflected field obtained from Monte Carlo simulations of the modal series representation (63) (solid curves), and the asymmetric (short dashed curve) and symmetric (dotted curve) Gaussian distributions

$$F(\tau) \approx 1 - \frac{1}{2} p(\alpha) \operatorname{erfc}\left(\frac{\tau}{\sqrt{2}}\right), \quad 0 < \tau < \infty$$

$$\approx \left[1 - \frac{1}{2} p(\alpha)\right] \operatorname{erfc}\left(-\frac{\tau}{\sqrt{2}}\right), \quad -\infty < \tau < 0 \quad (66)$$

$$F(\zeta) = \frac{1}{2} + \frac{1}{2} \operatorname{erf}\left(\frac{\zeta}{\sqrt{2}}\right), \quad -\infty < \zeta < \infty. \quad (67)$$

Fig. 15 used 500 modes; 100 modes at each end of the interval are beyond the sampled frequency range. Fig. 16 used 1000 modes; 200 modes at each end of the interval are beyond the sampled frequency range. The agreement is reasonably good. The “kink” discrepancy in Fig. 15 is caused by the discontinuity of the density function (64) at $\tau = 0$. The single mode approximate distribution $F(r_{in})$ (23) can be transformed by means of the quadratic relation $r_{in} = (\sqrt{\tau^2 + 4\alpha} + \tau)^2 / (4\alpha)$ to a dis-

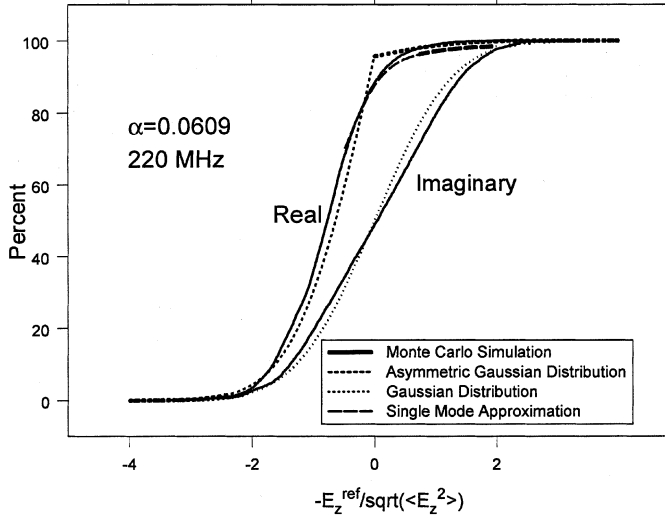


Fig. 15. Normalized reflected field from simulation and simple fit at $\alpha \approx 0.0609$ (220 MHz).

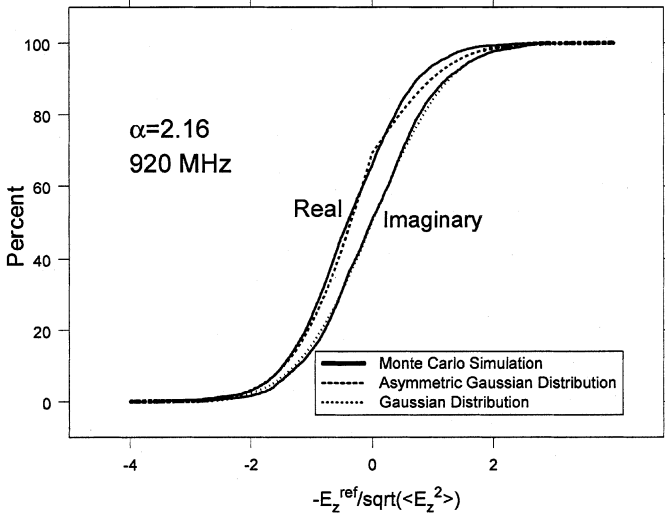


Fig. 16. Normalized reflected field from simulation and simple fit at $\alpha \approx 2.16$ (920 MHz).

tribution for the normalized real reflected field, for small values of τ in the undermoded limit

$$F(\tau) \approx 1 - \frac{4\alpha}{\pi} \sqrt{\frac{2}{\pi}} \left/ \left(\sqrt{\tau^2 + 4\alpha} + \tau \right) \right., |\tau| \ll 1, \alpha \ll 1. \quad (68)$$

This simple approximate distribution indicates how the “kink” should be interpolated as shown by the long dashed curve in Fig. 15. The short dashed curves in Figs. 13 and 14 show the improvement in the power balance distributions by use of this asymmetric Gaussian distribution (representing the limited bandwidth of the resonances). The long dashed curve in Fig. 13 shows the single mode approximate distribution (23) at the “kink” discrepancy.

The exponential decays of the density functions extracted in the asymptotic analyzes are all reproduced by the power balance results. One might be tempted to use the asymmetrical Gaussian distribution (66) to refine the extreme curves (59) and (60), instead of basing these on the symmetrical three sigma

point $M_0 = 3$. However, when the distributions are over-sampled in frequency, such that the resonances are fully resolved (for example the 220 MHz data), the extreme values must be determined from the confidence levels associated with the number of independent modes contained within the frequency sweep, as discussed in (27). Thus, the use of the symmetrical estimate is appropriate for the extremes, when the data is over-sampled in frequency, but it is inappropriate for the midrange distribution.

IX. CONCLUSION

The input impedance of a linear antenna inside a high Q , electrically large cavity has been investigated theoretically and experimentally. Monte Carlo simulations based on a modal series representation, with statistical estimates for modal spacing and eigenfunction amplitudes, are found to agree with measurements in a mode stirred chamber cavity. The parameter $\alpha = k^3 V / (2\pi Q)$, equal to the ratio of modal width to modal spacing, determines the magnitude of the impedance variations; the undermoded limit (separated, distinct modal spectra) $\alpha \ll 1$ results in large variations; the overmoded limit (many overlapping modes) $\alpha \gg 1$ results in small variations. Asymptotic analysis of the modal series yields formulas for the extreme values of the impedance. The modal series for an electrically short antenna has been shown to approximately represent resonant dipoles and wall-mounted monopoles, provided the local impedance and free space radiation resistance parameters are appropriately modified. The half space correlation function used for the monopole was shown to represent the known 3 dB normal field enhancement near the cavity wall. A simplified model based on balance of power gives practically useful simple formulas for the impedance distributions and the extreme values.

APPENDIX FIELD REPRESENTATION

This section briefly summarizes the potential and field representations [4], [5] (derivations can be found in [1]), introduces the difference potential that is convenient for treating thin antennas, and gives the impedance formula which uses these representations. Using potentials with time dependence $e^{-i\omega t}$, the electric field is

$$\underline{E} = i\omega \underline{A} - \nabla\phi \quad (69)$$

where in the Coulomb gauge $\nabla \cdot \underline{A} = 0$. Using a modal series for the cavity field [4], [5], [1], we can write

$$\begin{aligned} \underline{A}(\underline{r}) &= -\frac{1}{\epsilon_0 V} \sum_n \frac{\{1 + (1+i)/Q\}}{\omega^2 \{1 + (1+i)/Q\} - \omega_n^2} \\ &\quad \cdot \underline{A}_n(\underline{r}) \int_V \underline{A}_n(\underline{r}') \cdot \underline{J}(\underline{r}') dV' \\ &\approx -\frac{1}{\epsilon_0 V} \sum_n \frac{\underline{A}_n(\underline{r}) \int_V \underline{A}_n(\underline{r}') \cdot \underline{J}(\underline{r}') dV'}{\omega^2 (1+i/Q) - \omega_n^2} \end{aligned} \quad (70)$$

where \underline{J} is the antenna current, we have assumed Q is large in the last expression, and the neglect of $O(i/Q)$ terms in the numerator of (70) is justified here, because the frequency spacing between modes is assumed to be much smaller than

the frequencies of interest in this paper. The representation (70) is derived in [1] and in [5] (where the solenoidal electric field modes are proportional to the vector potential modes), and is similar to that found in [4] when the frequency approaches an eigenfrequency. The modal potentials satisfy the Helmholtz equation $(\nabla^2 + k_n^2) \underline{A}_n = 0$, the gauge condition $\nabla \cdot \underline{A}_n = 0$, the boundary condition $\underline{n} \times \underline{A}_n = 0$, the normalization $(1/V) \int_V \underline{A}_n \cdot \underline{A}_m dV = \delta_{nm}$, where $k_n = \omega_n/c$, c is the vacuum velocity of light, and ω_n are the eigenfrequencies of the simply connected, perfectly conducting, cavity. The quality factor Q is defined by

$$Q = \frac{\omega \mu_0 \int_V \underline{H}_n \cdot \underline{H}_n dV}{R_s \oint_S \underline{H}_n \cdot \underline{H}_n dS} \quad (71)$$

where the cavity boundary surface is S , the surface resistance is $R_s = 1/(\sigma\delta)$, the skin depth is $\delta = \sqrt{2/(\omega\mu\sigma)}$, μ and σ are the magnetic permeability and electric conductivity of the wall, and the modal magnetic field is $\mu_0 \underline{H}_n = \nabla \times \underline{A}_n$. The quality factor depends on ω but is expected to be weakly dependent on n , especially for large n (at least for the majority of modes).

Because we wish to consider linear antennas with small radius (and initially small length) it is convenient to improve the convergence of the modal series by subtracting out the quasistatic limit $\omega \rightarrow 0$ of the series (the form of the current is left untouched by this process, so in the electrically longer antenna it is not the quasistatic distribution)

$$\begin{aligned} \underline{A}(\underline{r}) - \underline{A}_s(\underline{r}) &= -\frac{1}{\varepsilon_0 V} \sum_n \frac{\omega^2 (1+i/Q) / \omega_n^2}{\omega^2 (1+i/Q) - \omega_n^2} \underline{A}_n(\underline{r}) \int_V \underline{A}_n(\underline{r}') \cdot \underline{J}(\underline{r}') dV' \\ &\approx -\frac{1}{\varepsilon_0 V} \sum_n \frac{\omega^2 / \omega_n^2}{\omega^2 (1+i/Q) - \omega_n^2} \underline{A}_n(\underline{r}) \int_V \underline{A}_n(\underline{r}') \cdot \underline{J}(\underline{r}') dV' \end{aligned} \quad (72)$$

where the quasistatic limit is

$$\begin{aligned} \underline{A}_s(\underline{r}) &= \frac{1}{\varepsilon_0 V} \sum_n \frac{1}{\omega_n^2} \underline{A}_n(\underline{r}) \int_V \underline{A}_n(\underline{r}') \cdot \underline{J}(\underline{r}') dV' \\ &\approx \frac{\mu_0}{4\pi} \int_V \frac{\underline{J}_s(\underline{r}') dV'}{|\underline{r} - \underline{r}'|} \\ &\approx \frac{\mu_0}{4\pi} \int_V \frac{\underline{J}(\underline{r}') dV'}{|\underline{r} - \underline{r}'|} - \nabla \nabla \cdot \frac{\mu_0}{8\pi} \int_V \underline{J}(\underline{r}') |\underline{r} - \underline{r}'| dV' \end{aligned} \quad (73)$$

where \underline{J}_s is the solenoidal part of the current. The approximations used in (73) ignore the boundary images of the source current and should be reasonably accurate if the region occupied by the antenna current is small compared to the cavity volume, the antenna is not near the boundary (except in the monopole case where we include the image in the wall where it is mounted), and the observation point is near the antenna. For the linear antenna

of radius a and length $2h$, with current $J_z = I(z)\delta(x)\delta(y)$, these become

$$A_z(a, z) - A_{sz}(a, z) = -\frac{1}{\varepsilon_0 V} \sum_n \frac{\omega^2 (1+i/Q) / \omega_n^2}{\omega^2 (1+i/Q) - \omega_n^2} \cdot A_{nz}(z) \int_{-h}^h A_{nz}(z') I(z') dz' \quad (74)$$

$$A_{sz}(a, z) \approx \frac{\mu_0}{4\pi} \left[\int_{-h}^h I(z') \frac{dz'}{\sqrt{a^2 + (z - z')^2}} - I(z) \right]. \quad (75)$$

The scalar potential in the Coulomb gauge can be taken as

$$\begin{aligned} \phi(\underline{r}) &= \frac{1}{\varepsilon_0 V} \sum_n \frac{1}{\eta_n^2} \phi_n(\underline{r}) \int_V \phi_n(\underline{r}') \rho(\underline{r}') dV' \\ &\approx \frac{1}{4\pi\varepsilon_0} \int_V \frac{\rho(\underline{r}') dV'}{|\underline{r} - \underline{r}'|} \end{aligned} \quad (76)$$

where the modal potentials again satisfy the Helmholtz equation $(\nabla^2 + \eta_n^2) \phi_n = 0$, the boundary condition $\phi_n = 0$, and normalization $(1/V) \int_V \phi_n \phi_m dV = \delta_{nm}$, where η_n are the eigenvalues of the simply connected, perfectly conducting, cavity. The final approximation in (76) again ignores images in the cavity boundary. Using the continuity equation $\nabla \cdot \underline{J} = i\omega\rho$ gives $\partial I / \partial z = i\omega q$, where q is the charge per unit length on the linear antenna. Thus, on the antenna we have

$$\begin{aligned} \phi(a, z) &\approx \frac{1}{4\pi\varepsilon_0} \int_{-h}^h \frac{q(z') dz'}{\sqrt{a^2 + (z - z')^2}} \\ &= \frac{1}{i\omega\varepsilon_0 4\pi} \int_{-h}^h \frac{\partial I}{\partial z'}(z') \frac{dz'}{\sqrt{a^2 + (z - z')^2}}. \end{aligned} \quad (77)$$

The antenna impedance is then found by using the stationary EMF representation [6]

$$Z_{in} = -\frac{1}{I^2(0)} \int_V \underline{E} \cdot \underline{J} dV = -\frac{1}{I^2(0)} \int_{-h}^h E_z(z) I(z) dz. \quad (78)$$

A. Short Dipole

The modal series field representation (70) for a short dipole in a cavity is

$$\begin{aligned} E_z &\approx -\frac{\partial}{\partial z} \phi - \frac{i\omega}{\varepsilon_0 V} \sum_n \frac{A_{nz}(\underline{r}) \int_V A_{nz}(z') I(z') dz'}{\omega^2 (1+i/Q) - \omega_n^2} \\ &\approx -\frac{\partial}{\partial z} \phi - \frac{i\omega h}{\varepsilon_0 V} I(0) \sum_n \frac{A_{nz}(\underline{r}) A_{nz}(0)}{\omega^2 (1+i/Q) - \omega_n^2} \end{aligned} \quad (79)$$

and the difference field from (74) is

$$\begin{aligned} E_z - E_{sz} &= i\omega (A_z - A_{sz}) \\ &\approx -\frac{i\omega I(0)h}{\varepsilon_0 V} \sum_n \frac{A_{nz}^2(0) \omega^2 / \omega_n^2}{\omega^2 (1+i/Q) - \omega_n^2}. \end{aligned} \quad (80)$$

Ignoring the scalar potential contribution in (79), since this term will have negligible contribution over most of the volume, we find

$$\begin{aligned} \langle |E_z|^2 \rangle_V &= \frac{1}{V} \int_V |E_z|^2 dV \\ &\approx \frac{\omega^2 h^2}{3\epsilon_0^2 V^2} |I(0)|^2 \sum_n \frac{A_{nz}^2(0)}{|\omega^2(1 + i/Q) - \omega_n^2|^2}. \end{aligned} \quad (81)$$

The reflected field is written as

$$E_z^{\text{ref}} = E_z - E_z^{\text{rad}} = (E_z - E_{sz}) - (E_z^{\text{rad}} - E_{sz}) \quad (82)$$

where E_z^{rad} is the field radiated by the antenna in free space. The first term in parenthesis is (80) and the second term is found from the EMF expression (78) applied to a short dipole (the local quasistatic field in the second term is approximated as not including images in the cavity walls)

$$\begin{aligned} &-\frac{1}{I^2(0)} \int_{-h}^h \{E_z^{\text{rad}}(z) - E_{sz}(z)\} I(z) dz \\ &= Z_{\text{rad}} - Z = R_{\text{rad}} \sim \frac{\eta_0 (kh)^2}{6\pi} \\ &\approx -\frac{1}{I(0)} (E_z^{\text{rad}} - E_{sz}) h \end{aligned} \quad (83)$$

where Z_{rad} is the impedance of the dipole in free space and the local impedance Z is (3).

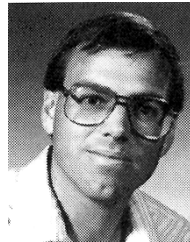
ACKNOWLEDGMENT

The authors would like to thank K. C. Chen of Sandia National Laboratories for many helpful discussions on the power balance section and T. H. Lehman for many helpful discussions regarding cavity mode statistics.

REFERENCES

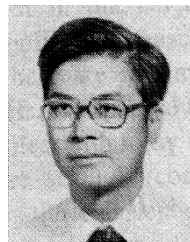
- [1] L. K. Warne, H. G. Hudson, W. A. Johnson, R. E. Jorgenson, S. L. Stronach of Sandia National Laboratories, and K. S. H. Lee of ITT Industries/AES, "Input impedance of antennas in high frequency cavities," Sandia Laboratories Report, SAND2000-3112, Dec. 2000.
- [2] D. A. Hill, "Linear dipole response in a reverberation chamber," *IEEE Trans. Electromagn. Compat.*, vol. 41, pp. 365–368, Nov. 1999.
- [3] P. R. Berman, Ed., *Cavity Quantum Electrodynamics*. New York: Academic, 1994.
- [4] W. R. Smythe, *Static and Dynamic Electricity*. Bristol, PA: Hemisphere, 1989, sec. 13.30, 13.32, and 13.17.
- [5] R. E. Collin, *Field Theory of Guided Waves*. New York: IEEE Press, 1991, sec. 5.9 and 5.10.
- [6] E. C. Jordan and K. G. Balmain, *Electromagnetic Waves and Radiating Systems*. Englewood Cliffs, NJ: Prentice-Hall, 1968, sec. 14.08, 14.09, 10.05, 10.07, 10.08, 14.05, and 14.06.
- [7] T. H. Lehman, "A statistical theory of electromagnetic fields in complex cavities," AFWL Interaction Note 494, May 1993.
- [8] R. H. Price, H. T. Davis, and E. P. Wenaas, "Determination of the statistical distribution of electromagnetic-field amplitudes in complex cavities," *Phys. Rev. E, Stat. Phys. Plasmas Fluids Relat. Interdiscip. Top.*, vol. 48, no. 6, Dec. 1993.
- [9] R. K. Chang and A. J. Campillo, Eds., *Optical Processes in Microcavities*. Singapore: World Scientific, 1996, pp. 389–426.
- [10] M. L. Mehta, *Random Matrices*. San Diego, CA: Academic, 1991, ch. 1.
- [11] M. C. Gutzwiller, *Chaos in Classical and Quantum Mechanics*. New York: Springer-Verlag, Inc., 1990, ch. 16, sec. 16.2, 16.3, 16.4, 16.7, 16.8, ch. 15 (sec. 15.5 and 15.6).
- [12] S. Deus, P. M. Koch, and L. Sirko, "Statistical properties of the eigenfrequency distribution of three-dimensional microwave cavities," *Phys. Rev. E, Stat. Phys. Plasmas Fluids Relat. Interdiscip. Top.*, vol. 52, no. 1, July 1995.

- [13] R. Balian and C. Bloch, "Distribution of eigenfrequencies for the wave equation in a finite domain. II. Electromagnetic field. Riemannian spaces," *Ann. Phys.*, vol. 64, pp. 271–307, 1971.
- [14] L. E. Reichl, *The Transition to Chaos*. New York: Springer-Verlag, 1992, ch. 8.
- [15] M. Brack and R. K. Bhaduri, *Semiclassical Physics*. Reading, MA: Addison-Wesley, 1997.
- [16] L. K. Warne and K. S. H. Lee, "Some remarks on antenna response in a reverberation chamber," *IEEE Trans. Electromagn. Compat.*, vol. 43, pp. 239–240, May 2001.
- [17] A. Papoulis, *Probability, Random Variables, and Stochastic Processes*. New York: McGraw-Hill, 1965, sec. 8-4, 14-1, pp. 126–127, 196–197, 189, 266–267.
- [18] I. S. Gradshteyn and I. M. Ryzhik, *Table of Integrals, Series, and Products*. New York: Academic, 1965, p. 316.
- [19] K. C. Chen and L. K. Warne, "Improved asymptotic expansions of time domain antenna current," *Radio Sci.*, vol. 26, no. 5, pp. 1205–1208, Sept./Oct. 1991.
- [20] L. B. W. Jolley, *Summation of Series*. New York: Dover, 1961, pp. 196–197, 104.
- [21] M. Abramowitz and I. A. Stegun, *Handbook of Mathematical Functions*. New York: Dover, 1972, p. 1026, 576.
- [22] S. A. Schelkunoff and H. T. Friis, *Antennas, Theory and Practice*. New York: Wiley, 1952, ch. 10, sec. 8.4, 8.13, 8.14, 8.15, 8.16, 13.14.
- [23] L. K. Warne and K. C. Chen, "A simple transmission line model for narrow slot apertures having depth and losses," *IEEE Trans. Electromagn. Compat.*, vol. 34, pp. 173–182, Aug. 1992.
- [24] J. M. Dunn, "Local, high-frequency analysis of the fields in a mode-stirred chamber," *IEEE Trans. Electromagn. Compat.*, vol. 32, pp. 53–58, Feb. 1990.



Larry K. Warne received the B.S.E.E. degree from Fairleigh Dickinson University, Teaneck, NJ, in 1976 and the M.S.E.E. and Ph.D. degrees from the California Institute of Technology, Pasadena, in 1977 and 1984, respectively.

Since 1978, he has been employed at Sandia National Laboratories, Albuquerque, NM, where he is currently a Distinguished Member of the Technical Staff.



Kelvin S. H. Lee received the B.S., M.S., and Ph.D. degrees in electrical engineering and applied sciences all from the California Institute of Technology, Pasadena, in 1960, 1961, and 1964, respectively.

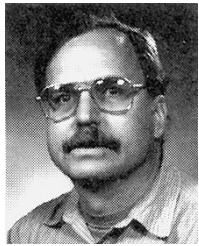
From 1965 to 1972, he was a Manager and Associate Director of the Electromagnetic and Laser Group, Northrop Corporate Laboratories, Pasadena, CA. From 1972 to 1982, he was a Senior Vice President of Dikewood Industries, Albuquerque, NM. From 1982 to 1998, he was a Vice President of Kaman Sciences Corporation, Santa Monica, CA.

Since 1998, he has been a Research Scientist with the Advanced Engineering and Sciences Division, ITT Industries, Los Angeles, CA, where he has been working on various problems in the field of electromagnetics.



H. Gerald Hudson was born in Pasadena, CA, in 1945. He received the A.A. degree as an Electronics Technician from Pasadena City College, Pasadena, CA, in 1965, the B.S.E.E. degree in electronics engineering from California State Polytechnic University, Pomona, in 1969, and the M.S. degree in electrical engineering from the University of Denver, Denver, CO, in 1970.

He is currently a Microwave Test/Measurement Engineer at Sandia National Laboratories, Albuquerque, NM.



William A. Johnson (M'00) was born in Beverly, MA, on April 26, 1951. He received the B.S., M.A., and Ph.D. degrees in mathematics, with minors in physics, from the University of Arizona, Tucson, in 1972, 1974, and 1978, respectively.

From 1978 to 1979, he was an Assistant Professor with the University of Mississippi, University, MS. From 1979 to 1981, he was with Science Applications, Inc. From 1981 to 1983, he was with Lawrence Livermore National Laboratories, Livermore, CA, operated by the University of California for the

U.S. Department of Energy. Since 1983, he has been with Sandia National Laboratories, Albuquerque, NM, where he is currently a Principal Member of the Technical Staff. He is also an adjunct Associate Professor for the Department of Mathematics at the University of New Mexico, Albuquerque.

Dr. Johnson is a Member of Commission B of the International Union of Radio Science.



Roy E. Jorgenson (S'86–M'88) was born in Portland, OR, on May 11, 1955. He received the B.S.E.E. degree from the University of Colorado, Boulder, in 1977 and the M.S. and Ph.D. degrees in electrical engineering from the University of Illinois at Urbana-Champaign, in 1985 and 1989, respectively.

He served as an Officer in the U.S. Army at Field Station Berlin, Berlin, Germany, until 1983. Since 1989, he has been with Sandia National Laboratories, Albuquerque, NM.



Stephen L. Stronach received the A.S.E.E.T. degree North American Technical Institute, Albuquerque, NM, in 1971.

Since 1971, he has been a Principal Technologist at Sandia National Laboratories, Albuquerque, NM, where in 1984, he joined the Electromagnetic Test Group and has worked primarily doing test automation programming, setup, and conduction.